

Article

Possible Formation Mechanism of Lunar Hematite

Yue Fu ¹, Huizi Wang ^{1,*}, Jiang Zhang ^{1,*}, Jian Chen ¹, Quanqi Shi ¹, Chao Yue ², Honglei Lin ³,
Ruiling Guo ¹, Anmin Tian ¹, Chao Xiao ¹ and Wensai Shang ¹

- ¹ Chinese Ministry of Education Key Laboratory of Particle Physics and Particle Irradiation, Shandong Provincial Key Laboratory of Optical Astronomy and Solar-Terrestrial Environment, Institute of Space Sciences, School of Space Science and Physics, Shandong University, 180 Wenhua Xilu, Weihai 264209, China
- ² Institute of Space Physics and Applied Technology, School of Earth and Space Sciences, Peking University, No. 5, Yiheyuan Road, Beijing 100871, China
- ³ Institute of Geology and Geophysics, Chinese Academy of Sciences, 19 Beitucheng West Road, Beijing 100029, China
- * Correspondence: whz@mail.sdu.edu.cn (H.W.); zhang_jiang@sdu.edu.cn (J.Z.)

Abstract: Hematite, a ferric mineral with diagnostic features in the visible and infrared spectral range, has recently been discovered in the polar regions of the Moon by the Chandrayaan-1 Moon Mineralogy Mapper (M³). The oxygen involving the oxidization process producing lunar hematite is supposed to originate from the Earth's upper atmosphere, and hematite with different ages may have preserved information on the oxygen evolution of the Earth's atmosphere in the past billions of years. The discovery of lunar hematite may provide insight into the understanding of the oxidation products on the Moon and other airless bodies. In this work, we analyze hematite abundance distribution in the lunar polar regions, showing that the content of hematite on the lunar surface increases with latitude, and is positively correlated with surface water abundance. We suggest that the latitude dependence of hematite is derived from the latitude dependence of water, which indicates that water may play an essential role in the formation of hematite. The correlation between hematite and the optical maturity parameter (OMAT) was analyzed and a significant positive correlation was observed, which suggests that the hematite in the polar regions is the result of gradual and persistent oxidation reactions. In addition, based on the analysis of oxygen particles in the Earth wind, it was found that O⁺ and O₂⁺ are much more abundant, suggesting that low-energy O⁺ or O₂⁺ ions escaping from the upper atmosphere of the Earth may play a crucial role in the formation of hematite in the lunar polar regions.

Keywords: lunar hematite; solar wind; Earth wind; lunar water; OMAT; oxygen particles



Citation: Fu, Y.; Wang, H.; Zhang, J.; Chen, J.; Shi, Q.; Yue, C.; Lin, H.; Guo, R.; Tian, A.; Xiao, C.; et al. Possible Formation Mechanism of Lunar Hematite. *Magnetochemistry* **2023**, *9*, 43. <https://doi.org/10.3390/magnetochemistry9020043>

Academic Editors: Chao Shen and Desheng Han

Received: 30 November 2022

Revised: 12 January 2023

Accepted: 18 January 2023

Published: 28 January 2023



Copyright: © 2023 by the authors. Licensee MDPI, Basel, Switzerland. This article is an open access article distributed under the terms and conditions of the Creative Commons Attribution (CC BY) license (<https://creativecommons.org/licenses/by/4.0/>).

1. Introduction

As a magnetic-field-weak and airless body, the Moon is directly irradiated by solar wind, Earth wind, and (micro)meteoroids. Understanding the formation processes of hematite on the Moon not only deepens our understanding of the interaction between solar/Earth wind and lunar surface, but also might be useful in ascertaining when the geomagnetic field arose, and has important scientific value for studying the evolution of the Earth-Moon system [1].

During about three-quarters of the lunar orbit, the Moon is immersed in the solar wind, which contains predominant protons, 1–5% alpha particles, and other heavy ions (oxygen abundance <0.1%) [2,3], depending on the solar wind speed, heliographic latitude, and solar cycle [4]. During the remaining 3–5 days of every lunar orbit, the Moon lies in the Earth's magnetosphere. When the Moon is in the magnetosphere, some terrestrial ions may be transported from Earth's upper atmosphere to the Moon, which is called "Earth wind" [1]. The Earth wind contains H⁺, O⁺, NO⁺, N⁺, and O₂⁺, and their relative proportions change dynamically with geomagnetic activity [5]. During the quiet period, H⁺ is dominant, while the proportion of O⁺ increases greatly during the magnetic storm [6–8].

Terada et al. (2017) [9] concluded that biogenic terrestrial oxygen has been transported to the Moon and implanted into the lunar regolith through analysis of 1–10 keV O^+ ion data from the Kaguya mission, which may have lasted for thousands of millions of years.

The bombardment of solar wind particles makes the lunar surface a highly reducing environment [10]. Previous studies have shown that minerals containing ferric iron (Fe^{3+}) are rare in lunar samples (less than 1%, and may be contaminants from the Earth) and the vast majority of iron on the Moon exists in the form of ferrous iron (Fe^{2+})-bearing minerals and metallic iron (Fe^0) due to the highly reducing environment [11]. In addition, several studies indicated that the solar wind also plays an important role in space weathering [12–15], which is a collection of complex physical and chemical processes [16]. Nanophase-iron ($np-Fe^0$) is a key product of space weathering, and its presence significantly changes the reflectance spectral characteristics of lunar soil [17]. It has been suggested that $np-Fe^0$ particles come from evaporation-deposition and solar wind reduction processes [18,19]. Furthermore, the optical maturity parameter (OMAT) mathematically derived from the reflectance of specific bands is considered to be robust for quantifying the spectral effects of space weathering [20], and it is negatively correlated with space weathering degree [21].

As the main components of the solar wind, the H^+ ion bombardment of the lunar soil can better explain the variation of the lunar surface OH/H_2O with the local time and latitude, so the bombardment of the solar wind can be regarded as the main exogenous source of lunar water [22]. Recent research has shown that when the Moon lies in the solar wind or Earth's magnetosphere, the surface OH/H_2O abundance in the polar region remains at the same level, which indicates that the ions in the Earth wind may also be the exogenous source of lunar surface hydration [23].

Recent studies have shown that, compared to the solar wind, the flux of oxygen particles is much higher in the Earth wind [3,9], which may promote the oxidization/oxyhydration processes. Li et al. (2020) [24] found the spectral absorption peak of hematite is around 850 nm (${}^4T_1 \leftarrow {}^6A_1$ charge transfer between Fe^{3+} and O^{2-}), which is less affected by pyroxene or other common minerals. The Moon Mineralogy Mapper (M^3) is a visible and near-infrared (0.5–3.0 μm) spectrometer aboard Chandrayaan-1. Through the study of the high-latitude M^3 datasets, the authors indicated that the absorption peak at 850 nm may represent the existence of hematite, and the integrated band depth between 750 nm and 1200 nm can characterize the relative concentration of hematite [24]. The oxygen from the Earth's upper atmosphere was possibly considered to be the oxidant in the hematite formation process, and the raw materials are ferrous iron or metallic iron on the lunar surface [24]. They proposed both anhydrous and aqueous formation mechanisms for hematite. The hematite can be formed by a hydrothermal reaction on the Earth, in which H_2O plays a significant role [25]. Honniball et al. (2022) [26] mapped the molecular water at high southern latitudes on the Moon and discovered a high-latitude water-bearing mineral host that may be a precursor to recently detected high-latitude hematite. Ferric iron-bearing phases were also confirmed to exist stably in the lunar materials according to the latest sample analyses on Chang'e-5 samples, which were collected from higher latitudes than Apollo samples [27,28]. Previous studies have shown that the IBDs (integrated band depth) of hematite have very weak latitudinal dependence [24]. Li et al. (2020) [24] proposed both aqueous and anhydrous mechanisms of hematite formation and pointed out that water can promote the reaction of the oxidation and oxyhydration processes but did not give specific evidence about it. In this study, we intend to further analyze the possible formation mechanisms of hematite. We modified the method of calculating the IBD of hematite and mapped hematite abundance in the lunar polar regions over a lunar cycle. Then we analyzed its correlation with surface OH/H_2O to reveal the role of water in the hematite formation process. We also analyzed the correlation between hematite and OMAT to show the relationship between hematite content and space weathering. At last, we discussed the possible oxygen particles participating in the lunar hematite formation process based on the current research near the Moon.

2. Materials and Methods

The M³ imaging spectrometer is a visible and near-infrared spectrometer aboard Chandrayaan-1, covering wavelengths between ~460 nm and 3000 nm. The M³ data were downloaded from the Planetary Data System (<http://pds-imaging.jpl.nasa.gov/data/m3/> (accessed on 29 June 2017)) [29]. We analyzed the data with latitudes above 70° within a lunation from 24 May 2009, to 21 June 2009, during which M³ has wider coverage [29]. We analyzed them in a lunar cycle due to the integrated band depth (IBD) data being affected by the observation conditions such as local time. The polar region was divided with a grid of 5° (longitude) × 15° (latitude) and we used the mean value in each subregion as the basis for characterizing the physical and chemical properties of the subregion.

2.1. The Hematite and Water Contents Derived from M³ Data

For the content of hematite, we used the method of Li et al. (2020) [24], proposing that the lower spectral reflectance at 850 nm corresponds to higher abundances of hematite, and we used the ISSD (integral of squared second derivatives) method to remove the M³ spectra with the high noise level. Since the absorption peak of pyroxene occurs near 950 nm, the widespread presence of pyroxene on the Moon may affect the IBD calculation of hematite. To reduce the influence of pyroxene on the results, we used the spectra in 750–1000 nm to calculate the IBD parameter as the relative content of hematite. It should be noted that since the hematite on the Moon is rare, its abundance on the Moon is not yet clear, and the corresponding relationship between the IBD and its absolute abundance requires further instrumental calibrations or research on returned samples. The IBD of hematite represents only the relative content of hematite, which is referred to as the content of hematite in this article. In Addition, the confidence interval (CI) error bars given in Figure 1a,b,e,h are calculated by $CI = \frac{\sigma}{\sqrt{n}} \times t_{n-1}$, where t_{n-1} is the t-distribution with n degree of freedom and σ is the standard deviation ($\sigma = 1.253 \times 10^4$ by the mean absolute deviation) [30].

We calculated the relative band depth H around 2.8 μm as an indicator of the lunar surface OH/H₂O abundance

$$H = 1 - R_b/R_c$$

where R_b is the average reflectance over channels of OH/H₂O absorption features between 2896 and 2936 nm, and R_c is the average reflectance over channels of 2617, 2657, and 2697 nm, representing the reflectance continuum [31]. Additionally, we used the probability of absorption depth of more than 0.05 and less than 0.2 as the index characterizing the OH/H₂O abundance level of the Moon [23]. The error in Figure 1c,d is calculated by $\epsilon = \frac{n}{N} \times (\frac{\sqrt{n}}{n} + \frac{\sqrt{N}}{N})$, where n is the number of pixels with an absorption depth greater than 0.05, and N is the number of pixels with an absorption depth less than 0.2 in each bin, such that the occurrence rate for each bin is $N_0 = n/N$. The Poisson error for the event number n is \sqrt{n} . Similarly, the Poisson error for the event number N is \sqrt{N} . Using the propagation of error analysis according to average deviations, the uncertainty of the normalized value for each bin is $\Delta N_0 = N_0 \sqrt{(\frac{\sqrt{n}}{n})^2 + (\frac{\sqrt{N}}{N})^2}$ ($2(\frac{\sqrt{n}}{n} \times \frac{\sqrt{N}}{N})$ close to zero). The error bar shown in Figure 1c,d is scaled by a factor of 10 [23].

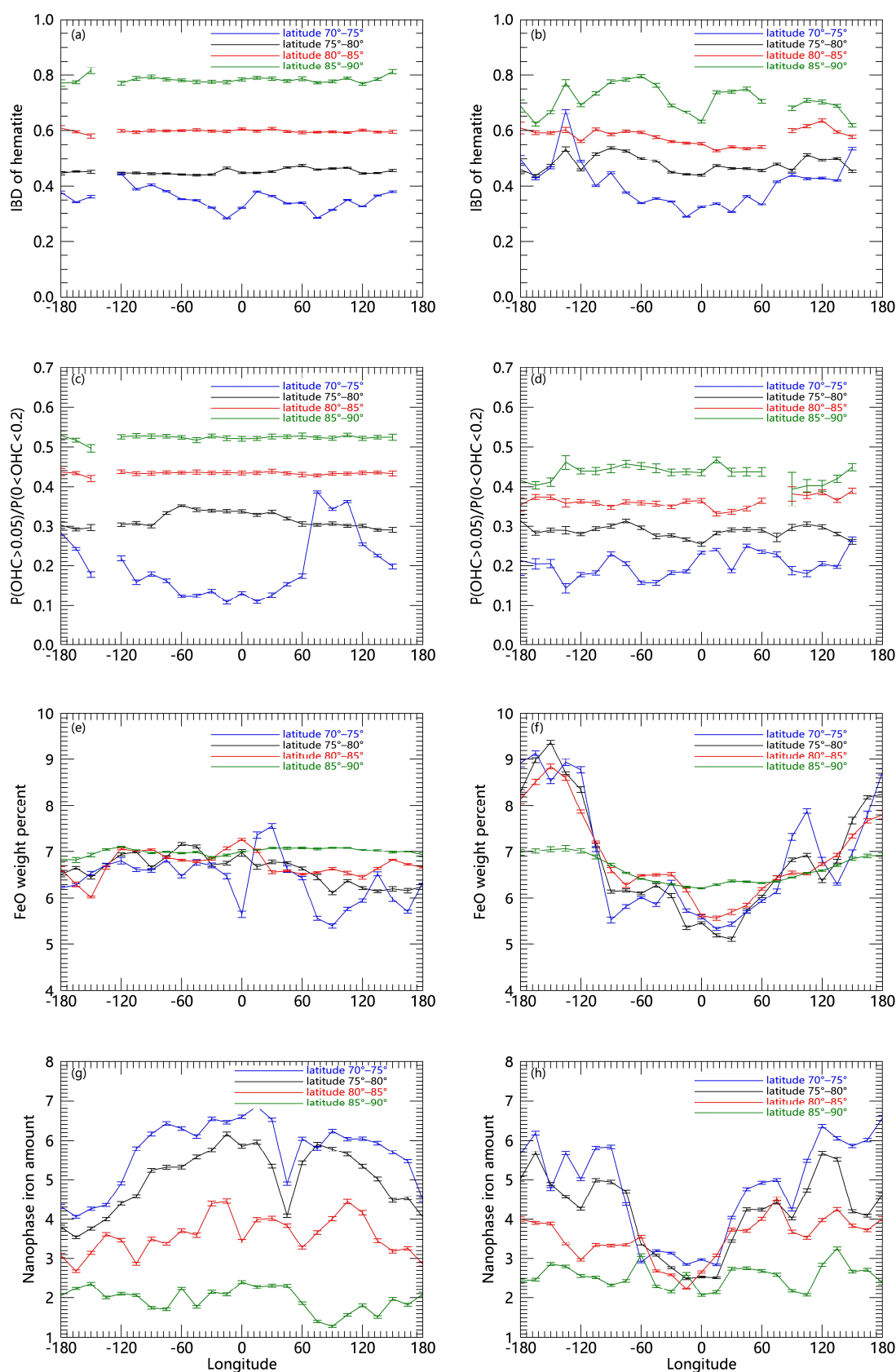


Figure 1. Content of different materials in the high latitudes of the Moon with a grid of 5° (longitude) \times 15° (latitude) and the mean value is used in each region. (a,b) The IBD of hematite. (c,d) The probability of $2.8 \mu\text{m}$ absorption depth between 0.05 and 0.2 represents the OH/H₂O abundance level. (e,f) FeO weight percent (g,h) Nanophase iron amount.

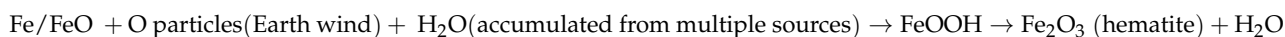
2.2. The Data of Ferrous Iron Abundance, Nanophase Metallic Iron Amount, and OMAT

We used the iron map derived from the Lunar Prospector measurements with a resolution of $0.5^\circ \times 0.5^\circ$ [32] as ferrous iron abundance data assuming that iron elements in lunar materials are dominated by ferrous iron. For the nanophase iron and OMAT data, we used the results calculated by Lemelin et al. (2022) [21] (<https://doi.org/10.5281/zenodo.5847000> (accessed on 13 May 2022)). They generated a gridded reflectance data cube from the Kaguya Spectral Profiler measurements for lunar polar regions and calibrated it to absolute reflectance using data from the Lunar Orbiter Laser Altimeter. They used this dataset to derive OMAT and nanophase iron abundance poleward of 50° N/S at a spatial resolution of 1 km pixel^{-1} .

3. Results and Discussion

Here we present the hematite, water, ferrous iron, and nanophase metallic iron abundances (Figure 1) obtained from the Chandrayaan-1 and Lunar Prospector datasets to discuss the possible formation processes of hematite involving the role of water. Figure 1 shows the mean content of different compounds in the high latitudes of the Moon with a grid of 5° (longitude) \times 15° (latitude). As shown in Figure 1a,b, we found that hematite content has a strong latitude dependence. The content of hematite increases with increasing latitude. The OH/H₂O concentration also increases with the increase in latitude (Figure 1c,d), which is consistent with the previous study [33]. The temperature in the higher latitudes is lower, and water will migrate toward the higher latitudes, which results in a tendency for water concentration to rise with increasing latitude. Then we calculated the variation of ferrous iron abundance in the high latitudes of the lunar surface (Figure 1e,f) but did not find a latitude dependence similar to that of hematite. We also used the data of the nanophase metallic iron amount calculated by Lemelin et al. (2022) [21] and analyzed the amount of nanophase iron in the high latitudes of the lunar surface (Figure 1g,h). The amount of nanophase iron decreases with increased latitude. At present, studies have shown that biogenic terrestrial oxygen has been transported to the Moon by the Earth wind and implanted into the surface of the lunar regolith [9]. Previous studies have shown that low-energy magnetospheric ions or protons are almost isotropic [34]. So we suggest that the oxygen particles injected into the lunar surface may be independent of the lunar latitude. Therefore, we suggest that the latitude dependence of hematite may be derived from the latitude dependence of water.

In order to reveal the role of water in the hematite formation, we also carried out the correlation analysis of hematite and water in the polar regions (Figure 2). The results show that there is an obvious positive correlation between the content of hematite and water concentration, and the correlation coefficient exceeds 0.9 in the north polar region and exceeds 0.85 in the south polar region, respectively. It indicates that water may play an essential role in the formation process of hematite. Current research indicates that water can promote the transformation of iron-oxygen phases ferrihydrite to hematite [35], and the presence of water can accelerate the crystallization of hematite through increased generation of nucleation sites. It was presumed that the proton transfer between OH groups is facilitated in the presence of water, which is required for the dehydration of ferrihydrite. Higher mobility of the ions accelerates the formation of hematite nuclei so that hematite can grow at a fast rate. Possible water-mediated chemical reactions are shown as follows [24]:



Whether the hematite was formed by a rapid process (such as large meteorite impact events) or accumulated through slow oxidation reactions is another question that needs to be discussed. In response to this problem, we analyzed the relationship between hematite content and OMAT. As shown in Figure 3, hematite content has a significantly positive correlation with OMAT. As mentioned before, space weathering is a collection of complex physical and chemical processes such as micrometeorite impacts, solar wind particle implantation, and cosmic ray irradiation. Micrometeorite impacts and cosmic ray

irradiation occur randomly. Solar wind particle implantation is currently considered to be an important process of space weathering. Allen et al. (1993) [36] inferred that when solar wind protons are implanted in the regolith, they may create a reducing environment during the impact. Considering that hematite will first transform into Fe²⁺-bearing minerals in a reducing environment [37,38], the positive correlation between the hematite and OMAT proves that the hematite content is related to the slow and persistent space-weathering effect. Another piece of evidence is that the hematite is pervasive in different polar regions rather than concentrated in a specific area. Hence, we infer that hematite is the result of slow and persistent oxidation reactions.

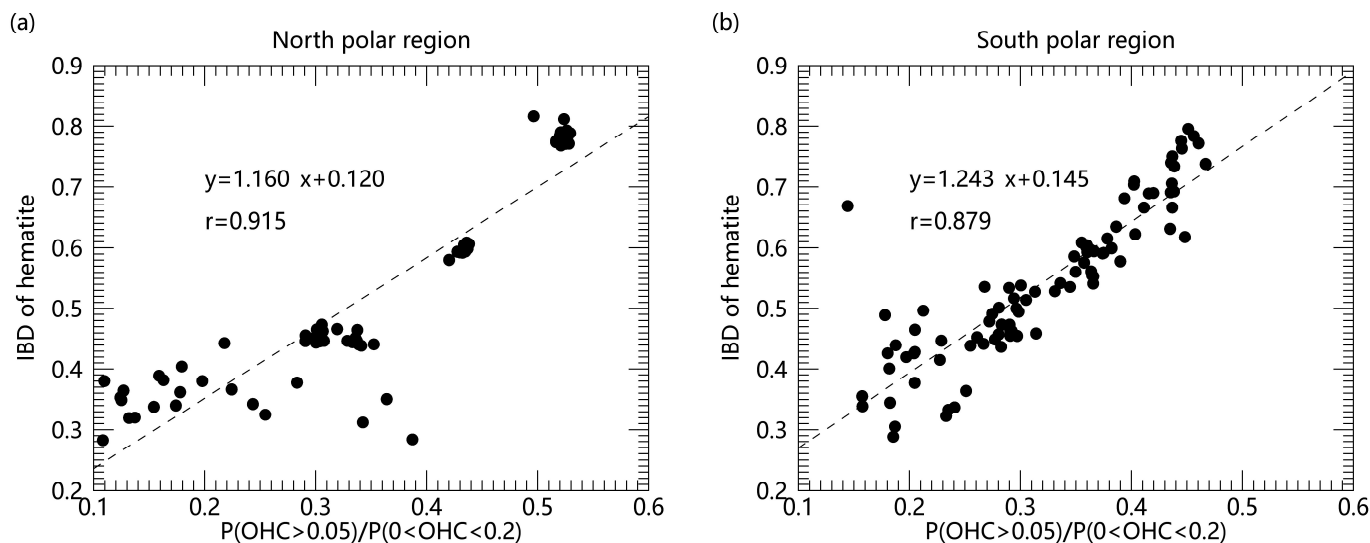


Figure 2. Comparison of hematite with water concentrations in the polar regions. ((a) north polar region (b) south polar region). The formulas in the figure show the result of linear regression fit and r in the figure represents the linear correlation coefficient with two variables.

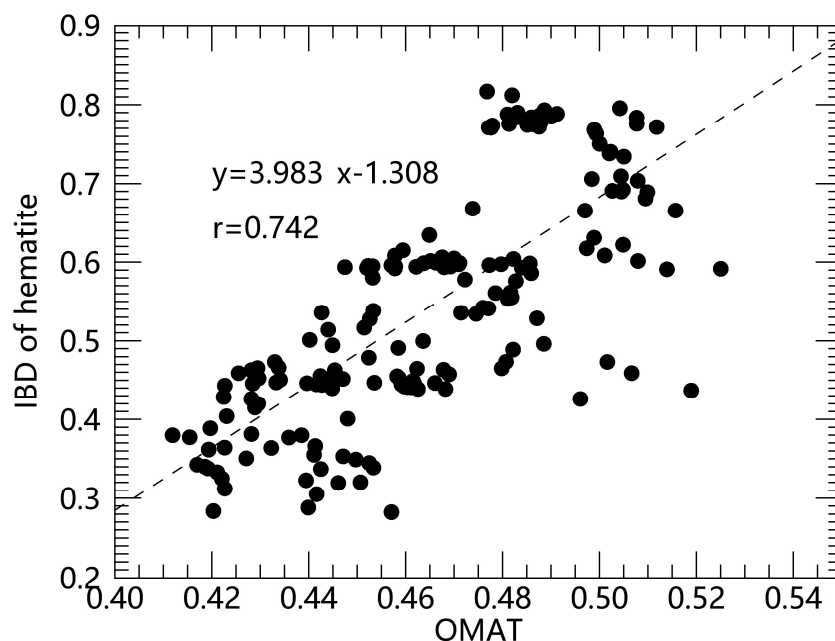


Figure 3. Comparison of hematite abundance with OMAT in the polar regions. The formulas in the figure show the result of linear regression fit and r in the figure represents the linear correlation coefficient with two variables.

In addition, we did not find a “ghost feature” in Figure 1. According to the previous simulation [39], there is a region that never received a full dose of the solar wind; for most of the orbit, this region is within the lunar wake and not directly exposed to the solar wind. Thus, it indicated more abundance of hematite; however, we did not find the region with a clear ghost feature. It can be explained by the essential role of water in the formation of hematite. The water on the Moon is formed by the bombardment of solar wind and Earth wind protons. The absence of “ghost features” further indicates that the formation of hematite requires the involvement of water.

The form of oxygen in the formation process of hematite also needs to be discussed. Considering the effect of solar wind hydrogen flux reducing hematite, we discuss the form of Earth wind oxygen particles reaching the Moon and their interaction with the lunar soil. Previous studies put the sputtering yield [amu ion⁻¹] as the basis of the yield of sputtering [40–42]. The main process by which energetic oxygen particles reach the lunar surface is sputtering, and hematite formation may need the injection of low-energy oxygen particles. We used SRIM to simulate oxygen ion bombardment of silica and found that the average sputtering yield of oxygen ions with about 0–300 eV is less than 1, which indicated a low sputtering level. For the lunar orbit or magnetosphere, as shown in Table 1, Terada et al. (2017) [9] found 1–10 keV O⁺ ions with a flux of at least 2.6×10^4 ions cm⁻² s⁻¹ from the Earth in lunar orbit by the Kaguya satellite data. Energetic O⁺ is also found in the distant magnetotail as a product of intense substorms [43]. According to the current research [44,45], the heavy ion fluxes (10^4 – 10^5 ions cm⁻² s⁻¹) with 32 atomic mass (O₂⁺) during geomagnetically disturbed times are found at lunar distances in the terrestrial magnetotail by the ARTEMIS data, which has a similar level with O⁺. The Two Wide-angle Imaging Neutral-atom Spectrometers (TWINS) can provide oxygen energetic neutral atom (ENA) imaging of the Earth’s magnetosphere [46]. The measurements show that the oxygen atoms of 16–128 keV at high-altitude emissions can reach 0.1 (eV cm² s sr)⁻¹, which can prove the existence of oxygen atoms in the magnetosphere [47]. Low-energy (10 eV to several hundred eV) oxygen atoms were found to outflow in the high-latitude magnetosphere for the flux of 2×10^3 to 4.1×10^3 (cm² s sr)⁻¹ [48]. However, there is no direct research showing that the oxygen atoms or oxygen molecules can be transported to the Moon in the Earth wind. Furthermore, previous studies have shown that the flux of oxygen ions to the Moon during the Earth’s geomagnetic storms and magnetosphere substorms can be increased by two orders of magnitude [49]. In conclusion, we infer that the oxygen particles in the hematite formation process are mainly low-energy oxygen ions or molecular oxygen ions during geomagnetically disturbed times. Aiming at the problem of the contribution of O⁺ and O₂⁺ in the hematite formation process, we should consider their efficiency of hematite formation, which consists of some unsolved problems; for example, comparison of their oxidizing properties and the best energy of the ions, which is similar to the Earth wind proton producing OH/H₂O: the main process of oxygen particles with high energy reaching the lunar surface is sputtering, and hematite formation may need the injection of low-energy oxygen particles.

Table 1. The form of oxygen in the Lunar orbit or magnetosphere.

Form	Energy Range	Flux	Position	Instrument	References
O ⁺	1–10 keV	More than 2.6×10^4 cm ⁻² s ⁻¹	Lunar orbit	Kaguya	[9]
O ₂ ⁺	1–10 keV	10^4 – 10^5 cm ⁻² s ⁻¹	Lunar orbit	ARTEMIS	[44]
O atoms	(1) 16–128 keV	(1) Less than 0.1 (eV cm ² s sr) ⁻¹	(1) magnetosphere	(1) TWINS	(1) [47]
	(2) 10 eV to several hundred eV	(2) 2×10^3 – 4.1×10^3 (cm ² s sr) ⁻¹ (outflow from the Earth)	(2) magnetosphere	(2) ILENA	(2) [48]
O ₂		No relevant research			

4. Conclusions and Perspective

Using the M³ visible and near-infrared spectroscopic data from Chandrayaan-1, we studied the relative concentration of hematite on the lunar surface and its formation mechanism. This study used integrated band depth (IBD) as the relative concentration of hematite following the method in Li et al. (2020) [24] and then analyzed the possible hematite formation process.

For the formation mechanism of hematite, we believe that hematite is formed by the oxidation of Fe-bearing minerals on the Moon, and the formation process may require the participation of OH/H₂O. It is the result of slow and persistent oxidation reactions simultaneously affected by the solar wind and the Earth wind.

The stable presence of hematite proves that not all regions of the lunar surface are highly reducing. In the high latitudes of the Moon, an oxidizing environment may exist in some regions due to less influence from the solar wind. Actually, in these regions, some oxidation reactions that we previously thought would not happen may occur, resulting in a wider variety of mineral species, which requires further research. The corresponding relationship between the integrated band depth (IBD) of hematite and the absolute concentration of hematite needs further in situ investigations.

Author Contributions: Data curation, Y.F., J.C.; Funding acquisition, J.Z., Q.S. and C.Y.; Investigation, Y.F.; Methodology, H.W., J.Z., J.C. and H.L.; Project administration, Q.S. and C.Y.; Resources, H.W. and Q.S.; Software, H.W., J.C. and H.L.; Supervision, J.Z., Q.S., and C.Y.; Visualization, Y.F.; Writing—original draft, Y.F.; Writing—review & editing, Y.F., H.W., J.Z., J.C., Q.S., C.Y., H.L., R.G., A.T., C.X. and W.S. All authors have read and agreed to the published version of the manuscript.

Funding: This research was supported by the National Key Research and Development Project (2019YFE0123300), National Natural Science Foundation of China (41974189, 41941001, 42225405), the National Key R&D Program of China 2020YFE0202100, NSFC research grant 42274200, 41974191 and China National Space Administration project D020303, the European Union's Horizon 2020 research and innovation program under grant agreement No. 871149.

Data Availability Statement: The hematite data required to generate the results used in this study are available online (https://figshare.com/articles/figure/Possible_formation_mechanism_of_lunar_hematite/21845592). This work has two corresponding authors (Correspondence to: Huizi Wang, whz@mail.sdu.edu.cn; Jiang Zhang, zhang_jiang@sdu.edu.cn) as this is an interdisciplinary work by space physics and planetary science teams.

Acknowledgments: We thank all the members of the Chandrayaan-1 M³ and Lunar Prospector instrument teams.

Conflicts of Interest: Authors declare no competing interests.

References

1. Ozima, M.; Seki, K.; Terada, N.; Miura, Y.N.; Podosek, F.A.; Shinagawa, H. Terrestrial Nitrogen and Noble Gases in Lunar Soils. *Nature* **2005**, *436*, 655–659. [[CrossRef](#)] [[PubMed](#)]
2. Hundhausen, A.J. Composition and Dynamics of the Solar Wind Plasma. *Rev. Geophys.* **1970**, *8*, 729–811. [[CrossRef](#)]
3. von Steiger, R.; Schweingruber, R.F.W.; Geiss, I.; Gloeckler, G. Abundance Variations in the Solar Wind. *Adv. Space Res.* **1995**, *15*, 3–12. [[CrossRef](#)]
4. Kasper, J.C.; Stevens, M.L.; Lazarus, A.J.; Steinberg, J.T.; Ogilvie, K.W. Solar Wind Helium Abundance as a Function of Speed and Heliographic Latitude: Variation through a Solar Cycle. *Astrophys. J.* **2007**, *660*, 901–910. [[CrossRef](#)]
5. Kronberg, E.A.; Ashour-Abdalla, M.; Dandouras, I.; Delcourt, D.C.; Grigorenko, E.E.; Kistler, L.M.; Kuzichev, I.V.; Liao, J.; Maggiolo, R.; Malova, H.V.; et al. Circulation of Heavy Ions and Their Dynamical Effects in the Magnetosphere: Recent Observations and Models. *Space Sci. Rev.* **2014**, *184*, 173–235. [[CrossRef](#)]
6. Yue, C.; Bortnik, J.; Li, W.; Ma, Q.; Wang, C.P.; Thorne, R.M.; Lyons, L.; Reeves, G.D.; Spence, H.E.; Gerrard, A.J.; et al. Oxygen Ion Dynamics in the Earth's Ring Current: Van Allen Probes Observations. *J. Geophys. Res. Space Phys.* **2019**, *124*, 7786–7798. [[CrossRef](#)]
7. Yue, C.; Bortnik, J.; Li, W.; Ma, Q.; Gkioulidou, M.; Reeves, G.D.; Wang, C.P.; Thorne, R.M.; Lui, A.T.Y.; Gerrard, A.J.; et al. The Composition of Plasma inside Geostationary Orbit Based on Van Allen Probes Observations. *J. Geophys. Res. Space Phys.* **2018**, *123*, 6478–6493. [[CrossRef](#)]

8. Fu, S.Y.; Wilken, B.; Zong, Q.G.; Pu, Z.Y. Ion Composition Variations in the Inner Magnetosphere: Individual and Collective Storm Effects in 1991. *J. Geophys. Res. Space Phys.* **2001**, *106*, 29683–29704. [[CrossRef](#)]
9. Terada, K.; Yokota, S.; Saito, Y.; Kitamura, N.; Asamura, K.; Nishino, M.N. Biogenic Oxygen from Earth Transported to the Moon by a Wind of Magnetospheric Ions. *Nat. Astron.* **2017**, *1*, 0026. [[CrossRef](#)]
10. Hapke, B. Space Weathering from Mercury to the Asteroid Belt. *J. Geophys. Res. Planets* **2001**, *106*, 10039–10073. [[CrossRef](#)]
11. Housley, R.; Blander, M.; Abdel-Gawad, M.; Grant, R.W.; Muir, A.H., Jr. Mössbauer Spectroscopy of Apollo 11 Samples. *Geochim. Cosmochim. Acta Suppl.* **1970**, *3*, 2251–2268.
12. Hemingway, D.J.; Garrick-Bethell, I.; Kreslavsky, M.A. Latitudinal Variation in Spectral Properties of the Lunar Maria and Implications for Space Weathering. *Icarus* **2015**, *261*, 66–79. [[CrossRef](#)]
13. Denevi, B.W.; Robinson, M.S.; Boyd, A.K.; Blewett, D.T.; Klima, R.L. The Distribution and Extent of Lunar Swirls. *Icarus* **2016**, *273*, 53–67. [[CrossRef](#)]
14. Trang, D.; Lucey, P.G. Improved Space Weathering Maps of the Lunar Surface through Radiative Transfer Modeling of Kaguya Multiband Imager Data. *Icarus* **2019**, *321*, 307–323. [[CrossRef](#)]
15. Blewett, D.T.; Denevi, B.W.; Cahill, J.T.S.; Klima, R.L. Near-UV and near-IR Reflectance Studies of Lunar Swirls: Implications for Nanosize Iron Content and the Nature of Anomalous Space Weathering. *Icarus* **2021**, *364*, 114472. [[CrossRef](#)]
16. Pieters, C.M.; Noble, S.K. Space Weathering on Airless Bodies. *J. Geophys. Res. Planets* **2016**, *121*, 1865–1884. [[CrossRef](#)] [[PubMed](#)]
17. Sasaki, S.; Nakamura, K.; Hamabe, Y.; Kurahashi, E.; Hiroi, T. Production of Iron Nanoparticles by Laser Irradiation in a Simulation of Lunar-like Space Weathering. *Nature* **2001**, *410*, 555–557. [[CrossRef](#)]
18. Anand, M.; Taylor, L.A.; Nazarov, M.A.; Shu, J.; Mao, H.K.; Hemley, R.J. Space Weathering on Airless Planetary Bodies: Clues from the Lunar Mineral Hapkeite. *Proc. Natl. Acad. Sci. USA* **2004**, *101*, 6847–6851. [[CrossRef](#)]
19. Noguchi, T.; Nakamura, T.; Kimura, M.; Zolensky, M.E.; Tanaka, M.; Hashimoto, T.; Konno, M.; Nakato, A.; Ogami, T.; Fujimura, A.; et al. Incipient Space Weathering Observed on the Surface of Itokawa Dust Particles. *Science* **2011**, *333*, 1121–1125. [[CrossRef](#)]
20. Lucey, P.G.; Blewett, D.T.; Taylor, G.J.; Hawke, B.R. Imaging of Lunar Surface Maturity. *J. Geophys. Res. Planets* **2000**, *105*, 20377–20386. [[CrossRef](#)]
21. Lemelin, M.; Lucey, P.G.; Camon, A. Compositional Maps of the Lunar Polar Regions Derived from the Kaguya Spectral Profiler and the Lunar Orbiter Laser Altimeter Data. *Planet. Sci. J.* **2022**, *3*, 63. [[CrossRef](#)]
22. Li, S.; Milliken, R.E. Water on the Surface of the Moon as Seen by the Moon Mineralogy Mapper: Distribution, Abundance, and Origins. *Sci. Adv.* **2017**, *3*, e1701471. [[CrossRef](#)]
23. Wang, H.Z.; Zhang, J.; Shi, Q.Q.; Saito, Y.; Degeling, A.W.; Rae, I.J.; Zong, Q.G.; Wei, Y.; Liu, J.; Guo, R.L.; et al. Earth Wind as a Possible Exogenous Source of Lunar Surface Hydration. *Astrophys. J.* **2021**, *907*, L32. [[CrossRef](#)]
24. Li, S.; Lucey, P.G.; Fraeman, A.A.; Poppe, A.R.; Sun, V.Z.; Hurley, D.M.; Schultz, P.H. Widespread Hematite at High Latitudes of the Moon. *Sci. Adv.* **2020**, *6*, eaba1940. [[CrossRef](#)] [[PubMed](#)]
25. Sun, W.; Huang, R.F.; Li, H.; Hu, Y.B.; Zhang, C.C.; Sun, S.J.; Zhang, L.P.; Ding, X.; Li, C.Y.; Zartman, R.E.; et al. Porphyry Deposits and Oxidized Magmas. *Ore Geol. Rev.* **2015**, *65*, 97–131. [[CrossRef](#)]
26. Honniball, C.I.; Lucey, P.G.; Arredondo, A.; Reach, W.T.; Malaret, E.R. Regional Map of Molecular Water at High Southern Latitudes on the Moon Using 6 Mm Data from the Stratospheric Observatory for Infrared Astronomy. *Geophys. Res. Lett.* **2022**, *49*, e2022GL097786. [[CrossRef](#)]
27. Mo, B.; Guo, Z.; Li, Y.; Zhu, D.; Zeng, X.; Li, X.; Liu, J.; Wu, Y. In Situ Investigation of the Valence States of Iron-Bearing Phases in Chang'E-5 Lunar Soil Using FIB, AES, and TEM-EELS Techniques. *At. Spectrosc.* **2022**, *43*, 53–59. [[CrossRef](#)]
28. Li, C.; Guo, Z.; Li, Y.; Tai, K.; Wei, K.; Li, X.; Liu, J.; Ma, W. Impact-Driven Disproportionation Origin of Nanophase Iron Particles in Chang'e-5 Lunar Soil Sample. *Nat. Astron.* **2022**, *6*, 1156–1162. [[CrossRef](#)]
29. Green, R.O.; Pieters, C.; Mouroulis, P.; Eastwood, M.; Boardman, J.; Glavich, T.; Isaacson, P.; Annadurai, M.; Besse, S.; Barr, D.; et al. The Moon Mineralogy Mapper (M3) Imaging Spectrometer for Lunar Science: Instrument Description, Calibration, on-Orbit Measurements, Science Data Calibration and on-Orbit Validation. *J. Geophys. Res. Planets* **2011**, *116*, E10. [[CrossRef](#)]
30. Kronberg, E.A.; Haaland, S.E.; Daly, P.W.; Grigorenko, E.E.; Kistler, L.M.; Fränz, M.; Dandouras, I. Oxygen and Hydrogen Ion Abundance in the Near-Earth Magnetosphere: Statistical Results on the Response to the Geomagnetic and Solar Wind Activity Conditions. *J. Geophys. Res. Space Phys.* **2012**, *117*, A12. [[CrossRef](#)]
31. Pieters, C.M.; Goswami, J.N.; Clark, R.N.; Annadurai, M.; Boardman, J.; Buratti, B.; Combe, J.P.; Dyar, M.D.; Green, R.; Head, J.W.; et al. Character and Spatial Distribution of OH/H₂O on the Surface of the Moon Seen by M3 on Chandrayaan-1. *Science* **2009**, *326*, 568–572. [[CrossRef](#)] [[PubMed](#)]
32. Lawrence, D.J.; Feldman, W.C.; Elphic, R.C.; Little, R.C.; Prettyman, T.H.; Maurice, S.; Lucey, P.G.; Binder, A.B. Iron Abundances on the Lunar Surface as Measured by the Lunar Prospector Gamma-Ray and Neutron Spectrometers. *J. Geophys. Res. Planets* **2002**, *107*, 13-1–13-26. [[CrossRef](#)]
33. Jones, B.M.; Aleksandrov, A.; Hibbitts, K.; Dyar, M.D.; Orlando, T.M. Solar Wind-Induced Water Cycle on the Moon. *Geophys. Res. Lett.* **2018**, *45*, 10,959–10,967. [[CrossRef](#)]
34. Harada, Y.; Futaana, Y.; Barabash, S.; Wieser, M.; Wurz, P.; Bhardwaj, A.; Asamura, K.; Saito, Y.; Yokota, S.; Tsunakawa, H.; et al. Backscattered Energetic Neutral Atoms from the Moon in the Earth's Plasma Sheet Observed by Chandrayaan-1/Sub-KeV Atom Reflecting Analyzer Instrument. *J. Geophys. Res. Space Phys.* **2014**, *119*, 3573–3584. [[CrossRef](#)]

35. Arinchtein, A.; Schmack, R.; Kraffert, K.; Radnik, J.; Dietrich, P.; Sachse, R.; Kraehnert, R. Role of Water in Phase Transformations and Crystallization of Ferrihydrite and Hematite. *ACS Appl. Mater. Interfaces* **2020**, *12*, 38714–38722. [[CrossRef](#)] [[PubMed](#)]
36. Allen, C.C.; Morris, R.V.; Lauer, H.V.; McKay, D.S. Microscopic Iron Metal on Glass and Minerals—A Tool for Studying Regolith Maturity. *Icarus* **1993**, *104*, 291–300. [[CrossRef](#)]
37. Sabat, K.C. Hematite Reduction by Hydrogen Plasma: Where Are We Now? *Int. J. Miner. Metall. Mater.* **2022**, *29*, 1932–1945. [[CrossRef](#)]
38. Jozwiak, W.K.; Kaczmarek, E.; Maniecki, T.P.; Ignaczak, W.; Maniukiewicz, W. Reduction Behavior of Iron Oxides in Hydrogen and Carbon Monoxide Atmospheres. *Appl. Catal. A Gen.* **2007**, *326*, 17–27. [[CrossRef](#)]
39. Tucker, O.J.; Farrell, W.M.; Poppe, A.R. On the Effect of Magnetospheric Shielding on the Lunar Hydrogen Cycle. *J. Geophys. Res. Planets* **2021**, *126*, e2020JE006552. [[CrossRef](#)]
40. Szabo, P.S.; Chiba, R.; Biber, H.; Stadlmayr, R.; Berger, B.M.; Mayer, D.; Mutzke, A.; Doppler, M.; Sauer, M.; Appenroth, J.; et al. Solar Wind Sputtering of Wollastonite as a Lunar Analogue Material—Comparisons between Experiments and Simulations. *Icarus* **2018**, *314*, 98–105. [[CrossRef](#)]
41. Szabo, P.S.; Biber, H.; Jäggi, N.; Brenner, M.; Weichselbaum, D.; Niggas, A.; Stadlmayr, R.; Primetzhofer, D.; Nenning, A.; Mutzke, A.; et al. Dynamic Potential Sputtering of Lunar Analog Material by Solar Wind Ions. *Astrophys. J.* **2020**, *891*, 100. [[CrossRef](#)]
42. Poppe, A.R.; Sarantos, M.; Halekas, J.S.; Delory, G.T.; Saito, Y.; Nishino, M. Anisotropic Solar Wind Sputtering of the Lunar Surface Induced by Crustal Magnetic Anomalies. *Geophys. Res. Lett.* **2014**, *41*, 4865–4872. [[CrossRef](#)]
43. Zong, Q.-G.; Wilken, B.; Woch, J.; Mukai, T.; Yamamoto, T.; Reeves, G.D.; Doke, T.; Maezawa, K.; Williams, D.J.; Kokubun, S.; et al. Energetic Oxygen Ion Bursts in the Distant Magnetotail as a Product of Intense Substorms: Three Case Studies. *J. Geophys. Res. Space Phys.* **1998**, *103*, 20339–20363. [[CrossRef](#)]
44. Poppe, A.R.; Fillingim, M.O.; Halekas, J.S.; Raeder, J.; Angelopoulos, V. ARTEMIS Observations of Terrestrial Ionospheric Molecular Ion Outflow at the Moon. *Geophys. Res. Lett.* **2016**, *43*, 6749–6758. [[CrossRef](#)]
45. Zhou, X.-Z.; Angelopoulos, V.; Poppe, A.R.; Halekas, J.S. ARTEMIS Observations of Lunar Pickup Ions: Mass Constraints on Ion Species. *J. Geophys. Res. Planets* **2013**, *118*, 1766–1774. [[CrossRef](#)]
46. McComas, D.J.; Allegrini, F.; Baldonado, J.; Blake, B.; Brandt, P.C.; Burch, J.; Clemmons, J.; Crain, W.; Delapp, D.; Demajistre, R.; et al. The Two Wide-Angle Imaging Neutral-Atom Spectrometers (TWINS) NASA Mission-of-Opportunity. *Space. Sci. Rev.* **2009**, *142*, 157–231. [[CrossRef](#)]
47. Valek, P.W.; Delmonico, E.; McComas, D.J.; Goldstein, J.; Allegrini, F.; Livi, S. Composition of 1–128 KeV Magnetospheric ENAs. *J. Geophys. Res. Space Phys.* **2018**, *123*, 2668–2678. [[CrossRef](#)]
48. Hesse, M.; Smith, M.F.; Herrero, F.; Ghielmetti, A.G.; Shelley, E.G.; Wurz, P.; Bochsler, P.; Gallagher, D.L.; Moore, T.E.; Stephen, T.S. Imaging Ion Outflow in the High-Latitude Magnetosphere Using Low-Energy Neutral Atoms. *Opt. Eng.* **1993**, *32*, 3153. [[CrossRef](#)]
49. Harnett, E.M.; Cash, M.; Winglee, R.M. Substorm and Storm Time Ionospheric Particle Flux at the Moon While in the Terrestrial Magnetosphere. *Icarus* **2013**, *224*, 218–227. [[CrossRef](#)]

Disclaimer/Publisher’s Note: The statements, opinions and data contained in all publications are solely those of the individual author(s) and contributor(s) and not of MDPI and/or the editor(s). MDPI and/or the editor(s) disclaim responsibility for any injury to people or property resulting from any ideas, methods, instructions or products referred to in the content.